NASA-CR-194777

University of Colorado at Boulder
Laboratory for Atmospheric and Space Physics
Space Technology Building
Campus Box 590
Boulder, Colorado 80309-0590

FINAL
IN-90-CR
OCIT.
198547
42 P

Evolution of Large-Scale Plasma Structures in Comets: Kinematics and Physics

NAGW-1387

FINAL REPORT

This project has achieved its original, major goal, viz., the delineation of the principal (or sole) mechanism for plasma-tail disconnection events (DEs). A DE involves the disconnection of the entire plasma tail from the head of the comet and the regrowth of a new tail following a more or less consistent morphology. The DE is probably the most spectacular event in cometary plasma physics.

The original approach of analyzing individual DEs in the IHW data set in order to determine the solar-wind conditions and thus, identify the principal mechanism, did not yield the anticipated result because of uncertainties in extrapolating solar-wind conditions to the comet. The raw materials, however, were an essential ingredient for the successful approach, viz., considering all of the Halley DEs as a group. In this approach, the uncertainties with individual DEs are minimized.

In situ solar-wind observations (from IMP-8, ICE, and PVO) and solar observations were used to synthesize the near-ecliptic variation of solar-wind speed, density, and dynamic pressure as well as the location of the heliospheric current sheet for the entire period of large-scale plasma activity.

Comparison of these solar-wind conditions with the times of DEs conclusively shows that the Halley DEs are associated with sector boundary crossings and not with any other property of the solar wind. This result was presented at the Asteroids, Comets, Meteors Meeting held in June at Belgirate, Italy. A copy of the paper, submitted to Planetary and Space Science, is attached. This paper covers 16 DEs observed in Halley's comet. A second paper covering all 19 major DEs is in preparation.

The interval of large-scale plasma activity in Halley's Comet (approximately November 1985 to May 1986) was excellent for the purposes of this investigation because of: (1) superb coverage of the comet through the IHW; (2) good in situ solar-wind measurements from several spacecraft (IMP-8, PVO, ICE, and Vega-1); and (3) heliospheric current-sheet data for all Carrington rotations from solar observations and potential field calculations (J.T. Hoeksema, Stanford University). No situation even close to this is foreseeable anytime in the near future.

This result, if the DEs in Halley's comet are representative, restricts DE mechanisms to those consistent with conditions at sector boundaries. To achieve acceptance, a DE mechanism must be reproducible in realistic MHD simulations.

(NASA-CR-194777) EVOLUTION OF LARGE-SCALE PLASMA STRUCTURES IN COMETS: KINEMATICS AND PHYSICS Final Report (Colorado Univ.) 42 p

N94-23251

Unclas

G3/90 0198547

To accomplish this, we have collaborated with Dr. Ray Walker (UCLA) and his associates. They are experts in cometary MHD simulations, have made their simulation programs available to us for modification, and have continued to consult with us. Dr. Walker extensively reviewed progress in November 1993. The results are very encouraging. Basically, magnetic reconnection on the sunward side of the comet produces DEs, but no other solar-wind changes seen during the comet Halley interval can. The general morphology and dynamics match the observed properties of DEs. An initial report on these results was presented by Yi and Brandt (BAAS 25, No. 3, p. 1066) at the October 1993 (Boulder, CO) meeting of the DPS/AAS. The observational results and the theoretical confirmation of sunward, magnetic reconnection as the principal mechanism for the DEs observed in Halley's comet will form a major part of the Doctoral Thesis for Mr. Yu Yi, Department of Physics, University of Colorado.

John C. Brandt
Principal Investigator

Date

Disconnection Events (DEs) and Sector Boundaries: The Evidence from Comet Halley 1985-1986

Y. Yi, F.M. Caputo, and J.C. Brandt

Laboratory for Atmospheric and Space Physics,

University of Colorado, Boulder, CO 80309

Received: _____; *Accepted:* _____

AAS WGAS macros v2.0

Abstract

Cometary and solar wind data from December 1985 through April 1986 are presented for the purpose of determining the solar wind conditions associated with comet plasma tail disconnection events (DEs). The cometary data are from *The International Halley Watch Atlas of Large-Scale Phenomena* (Brandt, Niedner, and Rahe, 1992). In addition, we present the kinematic analysis of 4 DEs, those of Dec. 13.5 and 31.2, 1985, and Feb. 21.7 and 28.7, 1986. The circumstances of these DEs clearly illustrate the need to analyze DEs in groups.

In situ solar wind measurements from IMP-8, ICE, and PVO were used to construct the variation of solar wind speed, density, and dynamic pressure during this interval. Data from these same spacecraft plus Vega-1 were used to determine the time of 48 current sheet crossings. These data were fitted to heliospheric current sheet curves (Hoeksema, 1989) extrapolated from the corona into the heliosphere in order to determine the best-fit source surface radius for each Carrington rotation.

Comparison of the solar wind conditions and 16 DEs in Halley's comet (the 4 DEs discussed in this paper and 12 DEs in the literature) leaves little doubt that DEs are associated primarily with crossings of the heliospheric current sheet and apparently not with any other property of the solar wind. If we assume that there is a single or primary physical mechanism and that Halley's DEs are representative, efforts at simulation should concentrate on conditions at current sheet crossings. The mechanisms consistent with this result are sunward magnetic reconnection (Niedner and Brandt, 1978) and tailward magnetic reconnection (Russell, Saunders, Phillips, and Fedder, 1986), if tailward reconnection can be triggered by the sector boundary crossing.

Subject headings: Comet–Solar Wind–Plasma Tail– Disconnection Event

1 Introduction

A. History of DEs

The first general scientific morphology of DEs was known to Barnard (1920) without any knowledge of the solar wind necessary to work toward a physical explanation. Biermann (1951) first established the existence of the solar wind by studying the plasma tails of comets. Later, Alfvén (1957) originated the basic picture of the cometary interaction with the interplanetary magnetic field (IMF). Alfvén proposed that the IMF would be captured and draped around the cometary ionosphere. About a decade later, Biermann, Brosowski, and Schmidt (1967) were the first to quantitatively study a comet/solar wind interaction model developed with the concept of a solar wind with frozen-in magnetic fields. The basic picture was confirmed by the six spacecraft flybys of comets Giacobini/Zinner and Halley in 1985-1986 (Neugebauer, 1990). However, one of the most spectacular phenomena of comets, the disconnection event (DE), where the plasma tail disconnects from the nucleus and subsequently flows away, remained unsolved. Niedner and Brandt (1978) made the first attempt to explain DEs. Since then, many theories (see Brandt, 1990) were suggested as explanations of DEs, but a fully self-consistent three-dimensional model for DEs does not yet exist. We can group the current competitive theories into two broad classes based on the triggering mechanisms: (1) pressure effects (e.g. Ip, 1980) and (2) magnetic reconnection. In the first class, the DEs occur through an interaction with a high-speed stream, a density enhancement, or an increase in the dynamic pressure of the solar wind. In the second class, the DEs occur through either tailward reconnection (Russell *et al.*, 1986) or sunward reconnection (Niedner and Brandt 1978).

B. Organization of Paper

The results presented here begin with the analysis of four DEs. These results strongly argue for the analysis of DEs in groups. We determine the variation of velocity, density, and dynamic pressure in the solar wind for the relevant time period from spacecraft measurements. The best-fit current sheet surface is determined by a fit to the spacecraft determinations of current sheet crossings. Finally, we compare the 16 DEs observed in comet Halley

to the solar wind conditions.

The basic concepts used in this work (such as co-rotation of solar wind properties) have been in the literature for years and are generally known. We find, however, that use of the "Carrington-Niedner Diagram" often requires explanation.

c. The "Carrington-Niedner Diagram"

Experience shows the best way to illustrate the relationship between DEs and the solar wind conditions is to display everything in one coordinate system referenced to a standard heliospheric distance, such as the Carrington longitude on the solar source surface. This can be done by corotating everything (e.g. comet Halley DE locations, solar wind observations, and the heliospheric sector boundaries) onto the Carrington longitude at the source surface. A solar wind source in the corona sends material into an archimedian spiral pattern if the sidereal pattern speed (14.4° per day) and the solar wind speed is constant. Then we can corotate solar wind features at the spacecraft (IMP-8, PVO, ICE, or Vega-1) to the coronal footprints of the archimedian spiral on the solar source surface. The same approach applies to the heliospheric neutral current sheet, calculated from a potential model (Hoeksema, 1989).

This approach to comparisons based on Carrington coordinate systems was originated by M.B. Niedner of the Goddard Space Flight Center. It was presented at the *20th ESLAB Symposium on the Exploration of Halley's Comet*, Heidelberg, Germany, October 1986 and subsequently published (Niedner and Schwingenschuh, 1987).

2 Analysis of Individual DEs

There have been many reports and analyses of DEs during comet Halley's 1985-1986 appearance. The list of the 16 comet Halley DEs and references to analyses and discussions are given in Table (1).

The detailed analysis of four DEs, two in December 1985 and two in February 1986, are given here. We determined the time of disconnection where possible by kinematic analysis. Otherwise, we used the kinematic properties of post-perihelion DEs, such as the rigorously-

examined DE of 1986 March 16.0 (Yi *et al.* 1993b), in order to calculate the disconnection time. Then we inferred the solar wind conditions from the corotated spacecraft solar wind measurements for each event. We then present the relationship between these DEs and the heliospheric current sheet (the sector boundary). This work is fully described by Yi *et al.* (1993a).

(a) 1985 Dec. 13.5 DE

The photographic images we used are listed in Table (2). A sequence of sample images is shown in Figure (1). The sector boundary was detected by Vega-1 (Dec 24.0) and PVO (Dec 29.0). The solar wind data are sparse around the time of the actual DE, but we can infer from the adopted velocity variation of this time period (see section 3) a solar wind speed of $\sim$ 370 km s^{-1} and a solar wind density of $\sim$ 15 cm^{-3}. The solar wind speed was lower than the average and the density was higher than the average at 1 AU. The sector boundary crossings by spacecraft, the heliospheric current sheet extrapolated from the corona, and the comet Halley DE locations are plotted in Figure (2). This DE occurred somewhat far from the heliospheric current sheet.

(b) 1985 Dec. 31.2 DE

Table (3) lists the photographs for this DE, and Figure (3) shows its evolution. The sector boundary was crossed by PVO (Dec 18.8), IMP-8 (Jan 4.8), ICE (Jan 5.6), and Vega-1 (Jan 10.0). IMP-8 measured the solar wind conditions for the sector boundary, where the solar wind speed was $\sim$ 400 km s^{-1} and the solar wind density was $\sim$ 10 cm^{-3}. The solar wind speed was decreasing slowly from a value of 700 km s^{-1} three days earlier. Comet Halley was coming out of the high-speed stream region. The solar wind speed was an average speed for 1 AU and the density was a little higher than average. Figure (4) shows the positions of the spacecraft sector boundary crossings and the DE, and the heliospheric current sheet. This DE's position was rather far from the projected sector boundary, but it is clear from the comparison with the spacecraft measurements that the heliospheric current sheet probably comes much closer to the DE than indicated.

(c) 1986 Feb. 21.7 DE

The photographs of this DE are described in Table (4), and are displayed in Figure (5). The sector boundary was detected by IMP-8 (Feb 11.0), ICE (Feb 13.0), and Vega-1 (Feb 16.0). As measured by IMP-8, the solar wind speed was $\sim$ 500 km s^{-1} and the solar wind density was $\sim$ 7 cm^{-3}. The solar wind speed was somewhat higher than the average and the density was average for 1 AU. Figure (6) illustrates the locations of the sector boundary, the spacecraft measurements, and the DEs. The DE occurred well away from the extrapolated sector boundary. However, comparison with the spacecraft observations indicates that the sector boundary is probably closer to the DE than indicated and perhaps the association with the sector boundary would be satisfactory.

(d) 1986 Feb. 28.7 DE

Table (5) lists the photographs analyzed for this DE, and samples are shown in Figure (7). The sector boundary was observed by PVO (Feb 6.8), and the geomagnetic index, ΣK_P (Feb 16.0). Plasma data from PVO show that the solar wind speed was $\sim$ 340 km s^{-1} and the solar wind density was $\sim$ 17-34 cm^{-3}. The density values are scaled to 1 AU. This density is much higher than the average solar wind density at 1 AU. Figure (8) displays the relationship between the heliospheric current sheet, the comet Halley DEs, and the spacecraft observations of the heliospheric current sheet crossings. The DE occurred quite close to the heliospheric current sheet. The solar wind speed was slower than average.

C. Need for Group Analysis

The apparent diversity of physical conditions for DEs illustrates the difficulty of analysis for individual DEs. The individual consideration of DEs does not allow a convincing selection between pressure effects or magnetic reconnection at the sector boundaries or any other candidate for the correct physical mechanism. Part of this difficulty may be attributed to corotation of the solar wind data, which assumes the constancy of the solar wind conditions for the Carrington rotation period, and to uncertainties in the current sheet calculations. In order to minimize the impact of uncertainties in any single event, we should study DEs as a group. This kind of effort has been started by Delva *et al.* (1991) and Brandt *et al.* (1992 a,b).

3 Solar Wind Velocity, Density, and Dynamic Pressure

A. Need for an Empirical Velocity Curve

In order to verify the cause of DEs, first we need to find the correlations between the DEs and conditions in the solar wind. To do this, we need full coverage of the solar wind velocity for the whole period under study. The solar wind velocity data curve is also the key for corotation of all other solar wind conditions (IMF structure, the solar wind density, and the dynamic pressure) as well as the solar wind velocity itself. This enables the comparison of DEs and solar wind properties on the Carrington-Niedner longitude diagrams as described above. Using the observational velocity data can reduce the errors as compared to simply assuming an average outflow velocity.

B. Data Sources, Approach, and Results

There were several spacecraft in orbit during the time period when DEs were observed on comet Halley. Those spacecraft are six comet Halley flyby missions (Giotto, Vega-1, Vega-2 Sakigake, Suisei, ICE), IMP-8 orbiting the earth, and PVO orbiting Venus.

We obtained solar wind data from IMP-8, PVO, and ICE. For consistency, we have used mostly IMP-8 data. However, IMP-8 has data gaps when it is inside the magnetosphere. We have augmented those times with data from PVO. Then, we have used ICE data as a supplement for still remaining data gaps. For the sector boundary observations, we added the Vega-1 sector boundary crossing times summarized by Delva *et al.*(1991).

The complete solar wind velocity curve is plotted in Figure (9 top) with the measurements from the different spacecraft plotted differently. We can see where the coverage is good and where the interpolation may influence the conclusions. In some cases, shift of data from different spacecraft might be appropriate and would reduce the fine structure. However we have not done this because such a procedure is ultimately subjective. By the same process, we can produce the variation of the solar wind plasma density in Figure (9 middle) and solar wind dynamic pressure in Figure (9 bottom). From Figure (9), we can see the changes of solar wind conditions and, when compared with the DEs (see Figure 15), their relationship

with the comet Halley DEs almost at a glance.

4 The Heliospheric Current Sheet

For the analyses, we used the heliospheric current sheet given by the potential field model (see Hoeksema, 1984). This model assumes that no currents flow near the sun; hence, the magnetic field can be described by a scalar potential field. A hypothetical spherical surface, called the source surface, is introduced at heights of 1.6 R_{SUN}, 2.0 R_{SUN}, and 2.5 R_{SUN} . At the the source surface, all magnetic field lines are assumed to be frozen in the plasma and are carried radial outward into the heliosphere by the solar wind. There are some disadvantages to the potential model, but for the large-scale phenomena the model is sufficient. This IMF structure (heliospheric current sheet) when projected to 1 AU is in reasonable agreement with the observations (Hoeksema, 1989).

For each of the Carrington rotations, the farther the source surface is located from the sun the less structure the current sheet exhibits. Specifically, as the source surface radius increases, the heliospheric current sheet remains closer to the projected solar equator for all Carrington longitudes. The heliospheric current sheet model dependency on the source surface radius is shown in Figure (10).

For each of the four spacecraft (IMP-8, PVO, ICE, Vega-1) we obtained the positions of the sector boundary crossing on the heliospheric source surface. Then we calculated the rms distance of the spacecraft from the sector boundary for each source surface radius (1.6 R_{SUN}, 2.0 R_{SUN}, and 2.5 R_{SUN}) for Carrington rotations 1769 to 1774. The 2.5 R_{SUN} source surface fit the spacecraft data best for Carrington rotations 1770 through 1774, while the 2.0 R_{SUN} source surface produced the lowest rms value for Carrington rotation 1769. However, in Carrington rotation 1769, the difference between the rms values for source surfaces of 2.0 R_{SUN} and 2.5 R_{SUN} was small. For all subsequent results quoted in this paper, we will use source surface 2.0 R_{SUN} for Carrington rotation 1769 and source surface 2.5 R_{SUN} for Carrington rotations 1770-1774. Figure (10) shows the sector boundary positions observed by spacecraft compared with the best-fit heliospheric current sheet.

For Carrington rotations 1769-1774, the four spacecraft crossed the sector boundaries a total of 48 times. The mean deviation between the spacecraft's location of the sector boundary and the position given by the potential field model was 6.7°, while the rms calculation of the dispersion was 8.9°. However, nearly 13% of the rms residue was produced by the 1986 March 17.7 Vega-1 detection of the sector boundary. If we neglect this crossing, the rms residue drops to 7.8°, while the mean residue decreases to 6.2°.

5 Comparison with the Halley DEs

A. The Heliospheric Current Sheet

Reference to investigations of the 16 obvious DEs used in this paper are given in Table (1). These DEs are overplotted on the best-fit heliospheric current sheet in Figure (11). Due to the retrograde motion of comet Halley, it detects one extra Carrington rotation than the Earth does. To model this we duplicated CR 1771. Since there were no DEs observed in this duplication period, the addition does not affect the results.

The association of DEs with sector boundaries seems clear. There is almost a one to one correspondence between sector boundary crossings and DEs, i.e., the number of opportunities for DE production at crossings is approximately equal to the observed number of DEs during this time interval. In addition, the distribution of errors with respect to the current sheet are similar for DEs and spacecraft determinations as shown in Figure (12).

Where there are gaps, they are consistent with the observing conditions. An excellent indicator of possible coverage is the histogram of images used in *The International Halley Watch Atlas of Large-Scale Phenomena* (Brandt, Niedner, and Rahe, 1992, p.707). Specifically, the coverage in late December 1985 and around perihelion (9 February 1986) is quite sparse. DEs that would be expected in these time periods probably were not observed.

We find a mean residue between the DEs' positions and the sector boundary of 11.3° and an rms value of 14.7°. The magnetic reconnection between the anti-parallel magnetic field lines draped around the comet ionosphere occurs over a period of time. Therefore, there should be a time delay between the comet encountering the heliospheric current sheet and

the observation of a DE for the sunward reconnection model. Niedner and Brandt (1978) estimated ~ 0.7 day. To account for this delay, we shifted each DE position an equal amount and found which shift produced the lowest rms residue. The lowest rms residue was 13.5° and occurred approximately at a 1 day shift.

Because the analysis of specific DEs, e.g., 1986 Jan. 9.7 (Niedner *et al.*, 1991) and 1986 Mar. 16.0 (Yi *et al.*, 1993b), suggests (by comparison with spacecraft measurements) that the major error might be in longitude, the results determined from seeking the closest current sheet location (which can involve a major latitude difference) may be in error. In essence, the point of minimum distance to the heliospheric current sheet may not be the actual place where the comet crossed the sector boundary. To consider this case, we calculated the distance between the DE and the position on the current sheet with the *same* (or approximately the same) heliospheric latitude as the DE. For no shift, the rms value was 19.2°. The minimum, 18.9°, occurred at approximately a 0.25-day shift of DE position. The difference between the best rms value of the shifted DE positions to that of no shift is only 0.3°. Hence, we do not believe this case can permit an accurate determination of the actual time between the comet penetration of the current sheet and the first visible onset of the DE. For consistency, we chose a 1-day shift of the DE positions, which produced an rms dispersion of 20.2°.

To test quantitatively whether DEs are associated with sector boundaries, we ran 5,000 cases of 16 DEs randomly placed on comet Halley's orbit for the time period between plasma tail turn-on and turn-off. There were two long periods where there were little or no observations. For calculating the random positions corresponding to the observation periods along comet Halley's orbit, we did not permit random positions in the observation periods of 1985 Dec 20-30 and 1986 Jan 20-Feb 20.

When we calculated the minimum distance to the current sheet with no latitude restriction, we obtained an rms value of 17.3°. Of these 5,000, iterations 90.9% were greater than the 13.5° which resulted from shifting the data by one day while 83.3% were greater than the 14.7° obtained from no shift. However, if we calculate the difference between the random DE positions and the current sheet with the *same* (or approximately the same) heliospheric

latitude, we obtain an rms value of 42.5°. Of the 5,000 iterations, 99.6% were greater than the rms result of 20.2° calculated by shifting the data, while 99.9% were larger than the rms result of 19.2° with no shift. The two cases are shown in Figures (13) and (14). We believe the physical situation lies between these two cases.

Quantitatively, the dispersion of the total samples around the best fit heliospheric current sheet is 8.9° for spacecraft determination and 13.5° for DEs. When the two worst cases are removed, the dispersions are 7.2° for spacecraft determinations and 10.0° for DEs. When the four worst cases are out, the dispersions are 6.4° for spacecraft determinations and 8.7° for DEs. These values seem to indicate a reasonable situation of the dispersion with respect to DEs being 35-40% higher than the dispersion with respect to spacecraft determinations.

B. The Solar Wind Velocity, Density, and Dynamic Pressure

Figure (15) shows the grand comparison of the DEs to the heliospheric current sheet (top panel), the solar wind velocity (second panel), density (third panel), and dynamic pressure (bottom panel).

If we count as a high-speed stream the periods when the solar wind speed is over 600 km s^{-1}, we find 11 high-speed streams for the total period of Carrington rotation 1769-1774. However, when the observational black-out periods are considered, this literally drops to 7 high-speed streams, but we count the number as 8 because the high-speed stream around Carrington longitude 233° of Carrington rotation 1771 is reasonably near the DE of 1986 Feb. 21.7. Further, only 6 out of 16 DEs are *anywhere near* the high-speed streams. There are simply not enough high-speed streams to do the job. Hence, the comparison to high-speed streams is not favorable.

There are many solar wind density changes with time. There are more than 22 instances of the solar wind density being greater than 20 cm^{-3}, and if the time of observational black-out is excluded, the number falls to 18. Only 10 DEs, however, are *anywhere near* density enhancements and the number drops to 8 DEs if we require that they lie within $\sim$ 24° in Carrington longitude. Finally, 6 DEs are *nowhere near* a density enhancement. Hence, the comparison with high-density regions is not favorable.

The solar wind dynamic pressure does not vary much because the solar wind density usually increases when the solar wind velocity decreases and vice versa. There are almost no strong increases of the dynamic pressure except in Carrington rotation 1771 when ground observations were not available. The only possible associations are with the 1985 Dec. 31.2 DE and the 1986 Feb. 21.7 DE. Therefore, the comparison with dynamic pressure effects is not favorable.

Besides the solar wind parameters discussed above, Yi *et al.* (1993a) considered the possible association of changes in the Alfvén Mach number with DEs and concluded that the association was unlikely. Finally, to assist in following the details of the various association with DEs, we have listed the Carrington longitude of each DE (determined by the adopted solar wind velocity curve) in Table (1).

6 Discussion and Conclusions

The association of DEs with sector boundaries seems to be very clear. Thus, the two possible mechanisms are sunward magnetic reconnection at the sector boundary (Niedner and Brandt 1978) and tailward magnetic reconnection due to sector boundary crossings (Russell *et al.* 1986), if sector boundaries can serve as triggers. If we assume that all DEs have a common cause and that the DEs in Halley's comet are representative, then future theoretical efforts must focus on conditions at sector boundaries.

The comet Halley interval was a good one in many respects, with intensive imaging from the ground, good heliospheric current sheet data, and solar wind data available from many spacecraft. Unfortunately, an opportunity similar to the comet Halley interval is not likely to occur anytime in the near future. While progress has been made, we have intensively analyzed only the DEs of comet Halley 1985-1986. Thus, continued work requires ground-based observations with proper coverage, solar wind measurements, *in situ* comet measurements, and theoretical studies. Future missions are critical for understanding of plasma structures and the solar wind interaction, as well as other areas of cometary physics.

The Ulysses mission will be a good chance to test the high-latitudinal variations of the

heliospheric current sheet and its relationship with cometary DEs. During the times of polar passage by Ulysses, we can gather cometary images, and correlate the cometary data with solar wind conditions as measured by Ulysses.

The field of global 3-dimensional magnetohydrodynamics (MHD) simulations has developed the ability to test the causalities and the processes of interaction between the solar wind and comets in response to changes in the solar wind. Schmidt-Voigt(1989) reported that he was unable to see the sunward magnetic reconnection morphology in response to the reversal of the IMF with an ideal MHD model. However, using a resistive MHD code adapted from Ogino, Walker and Ashour-Abdalla (1988), Yi and Brandt (1992) have produced the observed features of DE evolution, described by Brandt (1982), such as the symmetric ray formation and the disconnected tail, when an IMF reversal was simulated. Thus, we are optimistic that MHD simulations will ultimately reproduce the details observed in DEs.

Acknowledgements

Our work is largely based on the photographs archived by the Large Scale Phenomena Network (LSPN) of the International Halley Watch (IHW). We wish to express our sincere thanks to all observers around the world. We also thank solar wind data centers such as NSSDC for IMP-8 and ICE data and UCLA for PVO data.

REFERENCES

Alfvén, H., On the Theory of Comet Tails, *Tellus*, **9**, 92-96, 1957.

Barnard, E.E. , On Comet 1919b and on the Rejection of a Comets Tail, *Astrophys. J.*, bf 51, 102-106, 1920.

Biermann, L., Kometenschweife und Solar Korpuskularstrohlung *Zs. F. Astrophys.*, **29**, 279-286, 1951.

Biermann, L., B. Brosowski, and H.U. Schmidt, The Interaction of the Solar Wind with a Comet, *Solar Phys.*, **1**, 254-284, 1967.

Brandt, J.C., Observations and Dynamics of plasma tails, *Comets*, U. Arizona, Tucson, pp.519-537, 1982.

Brandt, J.C., The Large-Scale Plasma Structure of Halley's Comet, 1985-1986, *Comet Halley: Investigation, Results, Interpretation 1*, Ellis Horwood Ltd., pp.33-55,1990.

Brandt, J.C., M.B. Niedner, Jr., and J. Rahe, *The International Halley Watch Atlas of Large-Scale Phenomena*, LASP, U. Colorado, Boulder, 1992.

Brandt, J.C., C.E. Randall, Y. Yi, and M. Snow, Initial Overview of Disconnection Events in Halley's Comet 1986, *Asteroids, Comets, Meteors 1991*, LPI, Houston, pp.93-96, 1992a.

Brandt, J.C., F.M. Caputo, and Y. Yi, The Association of Disconnection Events (DEs) with Sector Boundaries: The Evidence from Comet Halley 1985-1986 *Bull. Am. Astron. Soc.*, **24**, 1270, 1992b.

Brosius, J.W., G.D. Holman, M.B. Niedner Jr., J.C. Brandt, J.A. Slavin, E.J. Smith, R.D. Zwickl, and S.J. Bame, On the Cause of Two Plasma Tail Disconnection Events in Comet Halley During the ICE-Halley Radial Period, *Astron. Astrophys.*, **187**, 267-275, 1987.

Celnik, W.E., P. Koczet, W. Schlosser, R. Schulz, P. Svejda, and K. Weißbauer, Structure and Dynamics of Plasma Tail Condensations of Comet P/Halley 1986, *Astron. Astrophys. Suppl.*, **72**, 89, 1988.

Delva, M., K. Schwingenschuh, M.B. Niedner, Jr., and K.I. Gringauz, Comet Halley Remote Plasma Tail Observations and In Situ Solar Wind Properties: VEGA-1/2 IMF/Plasma Observations ans Ground-based Optical Observations From 1 December 1985 to 1 May 1986, *Planet. Space Sci.*, **39**, 697-708, 1991.

Feldman, P.D., M.F. A'Hearn, M.C. Festou, L.A. McFadden, H.A. Weaver, and T.N. Woods, *Nature*, **324**, 433, 1986.

Hoeksema, J.T., Structure and Evolution of the Large-Scale Solar and Heliospheric Magnetic Field, Ph.D. Thesis, Stanford University, 1984.

Hoeksema, J.T., Extending the Sun's Magnetic Field through the Three-Dimensional Heliosphere, *Adv. Space Res.*, **9**, (4)141-(4)152, 1989.

Jockers, Observations of ions in comet P/Halley with a focal reducer, *Astron. Astrophys.*, **187**, 256-260, 1987.

Kubacek, D., E.M. Pittich, and J. Zvolankova, *ESA SP-250*, **III**, 277, 1986.

Lundstedt, H. and P.Magnusson, Two Disconnection Events in Comet P/Halley and Possible Solar Causes, *Astron. Astrophys.*, **187**, 261-263, 1987.

Neugebauer, M., Spacecraft Observations of the Interaction of Active Comets with the Solar Wind, *Reviews of Geophysics*, **28**, 231-251, 1990.

Niedner, M.B., Jr. and J.C. Brandt, Interplanetary Gas. XXIII. Plasma Tail Disconnection Events in Comets: Evidence for Magnetic Field Line Reconnection at Interplanetary Sector Boundaries?, *Astrophys. J.*, **223**, 655, 1978.

Niedner, M.B., Jr., J.C. Brandt, and Y. Yi, The 10 January 1986 Disconnection Event in Comet Halley, *Cometary Plasma Processes*, AGU, Washington, D.C., pp.153-159, 1991.

Niedner, M.B., Jr. and K. Schwingenschuh, Plasma-tail Activity at the time of the Vega Encounters, *Astron. Astrophys.*, **187**, 103-108, 1987.

Ogino, T., R.J. Walker, and M. Ashour-Abdalla, A Three-Dimesional MHD Simulation of the Solar Wind With Comet Halley, *J. Geophys. Res.*, **93**, 9568, 1988.

Russell, C.T., M.A. Saunders, J.L. Phillips, and J.A. Fedder Near-Tail Reconnection as the Cause of Cometary Tail Disconnections *J. Geophys. Res.*, **91**, 1417-1423, 1986.

Saito, T., K. Saito, T. Aoki, and K. Yumoto, Possible Models on Disturbances of the Plasma Tail of Comet Halley during the 1985-1986 apparition, *Astron. Astrophys.*, **187**, 201-208, 1987.

Schmidt-Voigt M., Time-dependent MHD simulations for Cometary Plasmas, *Astron. Astrophys.*, **210**, 433-454, 1989.

Tomita, K., T. Saito, and S. Minami, Structure and Dynamics of the Plasma Tail of Comet P/Halley I. Kink Event on January 10-11, 1986, *Astron. Astrophys.*, **187**, 215-219, 1987.

Yi, Y. and J.C. Brandt, A Preliminary 3D MHD Simulation of Cometary Plasma Tail Dynamics, *EOS Trans.*, **73**, 444, 1992.

Yi, Y., J.C. Brandt, M. Snow, and C.E. Randall, The Disconnection Events of 13-18 April 1986 and the Cessation of Plasma Tail Activity, *Astrophys. J.*, in press, 1993a.

Yi, Y., J.C. Brandt, C.E. Randall, and M. Snow, The Disconnection Event of Comet Halley on 16.0 March 1986, *Astron. J.*, submitted, 1993b.

Figure 1: Representative time sequence of photographs of a Disconnection Event in comet Halley from 13 to 15 December 1985, chosen from the Large Scale Phenomena Network (LSPN) data base of the International Halley Watch (IHW). From top to bottom: 18.80 UT on Dec. 13 by M. Jäger, Austria; 19.48 UT on Dec. 13 by F. Van Wyk, LSPN Island Network, Sutherland; 2.38 UT on Dec. 14 by R. Hill, Warner and Swasey Observatory, USA; 3.29 UT on Dec. 14 by E. Moore *et al.*, Joint Observatory for Cometary Research, USA; 1.22 UT on Dec. 15 by W. Liller, University of Michigan/CTIO, Chile.

Figure 2: Carrington-Niedner Diagram for the 13.5 December 1985 DE. Displayed are four spacecraft (IMP-8, ICE, PVO, and Vega-1) detections of the sector boundaries and the heliospheric current sheet position for source surface 2.0 R_{SUN} for Carrington rotation 1769. The + symbol marks ion tail turn-on position. The × represents a 1-day shift of the December 13.5 DE.

Figure 3: Representative time sequence of photographs of a Disconnection Event in comet Halley from 30 December 1985 through 1 January 1986. From top to bottom: 19.25 UT on Dec. 30, 1985 by A. Laugier, Observatory of Haute-Provence, France; 9.34 UT on Dec. 31, 1985 by H. Maehara, Kiso Observatory, Japan; 9.75 UT on Dec. 31, 1985 by H. Maehara, Kiso Observatory, Japan; 1.72 UT on Jan. 1, 1986 by G. Emerson, E.E. Barnard Observatory, USA.

Figure 4: Carrington-Niedner Diagram for 31.2 December 1985 DE. Displayed are four spacecraft (IMP-8, ICE, PVO, and Vega-1) detections of the sector boundaries and the heliospheric current sheet position for source surface 2.5 R_{SUN} for Carrington rotation 1770. The × represents a 1-day shift of the December 31.2 DE.

Figure 5: Time sequence of photographs of a Disconnection Event in comet Halley on 22 February 1986. From top to bottom: 3.02 UT on Feb. 22, 1986 by F. Van Wyk, LSPN Island Network, Sutherland; 18.70 UT on Feb. 22, 1986 by UKSTU, Royal Observatory, Australia.

Figure 6: Carrington-Niedner Diagram for 21.7 February 1986 DE. Displayed are four spacecraft (IMP-8, ICE, PVO, and Vega-1) detections of the sector boundaries and the heliospheric current sheet position for source surface 2.5 R_{SUN} for Carrington rotation 1771. The × represents a 1-day shift of the February 21.7 DE.

Figure 7: Representative time sequence of photographs of a Disconnection Event in comet Halley on 2 March 1986. From top to bottom: 0.00 UT on Mar. 2, 1986 by W. Liller, University of Michigan/CTIO, Chile; 11.76 UT on Mar. 2, 1986 by W. Liller, University of Michigan/CTIO, Chile; 12.04 UT on Mar. 2, 1986 by W. Liller, University of Michigan/CTIO, Chile.

Figure 8: Carrington-Niedner Diagram for 28.7 February 1986 DE. Displayed are four spacecraft (IMP-8, ICE, PVO, and Vega-1) detections of the sector boundaries and the heliospheric current sheet position for source surface 2.5 R_{SUN} for Carrington rotation 1772. The $\times$ represents a 1-day shift of the February 28.7 DE.

Figure 9: Variations of the solar wind conditions. From top to bottom: solar wind speed; solar wind density; solar wind dynamic pressure, where the unit was chosen with the density 8 cm^{-3} and the velocity 400 km sec^{-1}. The thin line is the IMP-8 data, the medium line is ICE data, and the thick line is PVO data.

Figure 10: Current Sheet fit to spacecraft data. Displayed are the four spacecraft (IMP-8, ICE, PVO, and Vega-1) detections of the sector boundary and the current sheet positions for source surface radii 2.0 R_{SUN} and 2.5 R_{SUN}. For clarity we have left off the 1.6 R_{SUN} source surface. The 2.5 R_{SUN} source surface can be identified as the curve typically closer to 0° latitude.

Figure 11: Comparison of comet Halley's 16 DEs to the best-fit current sheet. The solid curves depicts the 'best fit' current sheet as determined by the spacecraft data. The lightly-dashed curve represents comet Halley's orbit with each individual DE denoted by an asterisk. Ion tail turn-on/off and perihelion are marked by diamonds and a triangle respectively. The heavy dashed boxes correspond to periods with little or no observations of comet Halley. Due to the retrograde motion of comet Halley, we duplicated CR 1771.

Figure 12: Histograms of dispersion for DEs and spacecraft detections of the sector boundary.

Figure 13: Histogram in 1.0° bins of the rms dispersion of 5000 iterations of 16 DEs randomly placed along comet Halley's orbit as described in the text. The rms dispersion is for the case where we calculated the minimum distance between the current sheet and the DE. The dashed line is the actual rms dispersion (13.5°) of comet Halley's 16 DEs shifted approximately one day.

Figure 14: Histogram in 1.0° bins of the rms dispersion of 5000 iterations of 16 DEs randomly placed along comet Halley's orbit as described in the text. The rms dispersion is for the case where the DE and the current sheet have the same (or approximately the same) heliospheric latitude. The dashed line is the actual rms dispersion (22.2°) of comet Halley's 16 DEs shifted 1.0 day.

Figure 15: Grand Comparison Diagram: This is a composite plot of Fig.(9) and Fig.(11). From top to bottom: comet Halley's 16 DEs and the best-fit current sheet; solar wind speed; solar wind density; solar wind dynamic pressure.

DE No.	Disconnection Time (UT)	DE location CR, longitude	Analysis done	Related Reports
1	1985 Dec 4.7	1769,224.8°		Niedner (1986)
2	13.5	85.4°	This paper	Niedner (1986)
3	31.2	1770,182.8°	Saito *et al.*(1987)	Niedner (1986)
			This paper	
4	1986 Jan 8.6	54.3°		Niedner (1986)
				Kubacek *et al.*(1986)
5	9.7	36.0°	Niedner *et al.*(1991)	Niedner (1986)
				Tomita *et al.*(1987)
6	Feb 21.7	1771, 7.4°	This paper	Niedner (1986)
7	28.7	1772,248.7°	This paper	Niedner (1986)
8	Mar 4.5	184.1°		Niedner (1986)
				Celnik *et al.*(1988)
9	8.4	139.6°	Niedner&Schwingenschuh(1987)	Niedner (1986)
				Wu&Qiu (1987)
10	12.6	65.9°		Niedner (1986)
				Saito *et al.*(1987)
				Celnik *et al.*(1988)
11	16.0	31.4°	Yi *et al.*(1993b)	Feldman*et al.*(1986)
				Celnik *et al.*(1988)
12	19.3	1773,344.1°	Brosius *et al.*(1987)	Niedner (1986)
				Celnik *et al.*(1988)
13	Apr 1.7	155.4°		Celnik *et al.*(1988)
14	6.9	79.4°		Niedner (1986)
				Celnik *et al.*(1988)
15	10.9	45.5°	Brosius *et al.*(1987)	Brandt&Niedner(1986)
			Lundstedt & Magnusson (1987)	Jockers (1987)
				Celnik *et al.*(1988)
16	13.7	1774,348.7°	Lundstedt & Magnusson (1987)	Niedner (1986)
			Yi *et al.*(1993a)	Celnik *et al.*(1988)

Table 1: 16 DEs identified based on *The International Halley Watch Atlas of Large-Scale Phenomena* (Brandt, Niedner, and Rahe 1992).

Date	Hours (UT)	Distance (10^6 km)	Observer(s) Observatory	LSPN No.
1985 Dec 13	18.80	1.43	M. Jäger, Austria	
	19.20	1.56	F. Van Wyk, LSPN Island Network, Sutherland	1769
	19.48	1.60	F. Van Wyk, LSPN Island Network, Sutherland	1770
Dec 14	1.22	2.35	W. Liller, University of Michigan/CTIO, Chille	215
	1.67	2.39	W. Liller, University of Michigan/CTIO, Chille	216
	2.12	2.45	W. Liller, University of Michigan/CTIO, Chille	217
	2.38	2.50	R. Hill, Warner and Swasey Observatory, USA	2582
	2.60	2.54	W. Liller, University of Michigan/CTIO, Chille	218
	3.12	2.60	W. Liller, University of Michigan/CTIO, Chille	219
	3.29	2.65	E. Moore *et al.* Joint Obs.for Cometary Res., USA	1723
Dec 15	1.22	7.06	W. Liller, University of Michigan/CTIO, Chille	220
	2.09	7.39	W. Liller, University of Michigan/CTIO, Chille	222

Table 2: 1985 Dec 13.5 DE: Observation time, the calculated distance between the comet head and the end of the disconnected plasma tail, observatory and observers for the images 13 to 15 December 1985, archived in the Large Scale Phenomena Network (LSPN) data base of the International Halley Watch (IHW). In calculating the distance we have assumed that the disconnected plasma tail recedes along the prolonged radius vector.

Date	Hours (UT)	Distance (10^6 km)	Observer(s) Observatory	LSPN No.
1985 Dec 31	9.34	0.62	H. Maehara, Kiso Observatory, Japan	1620
	9.75	0.75	H. Maehara, Kiso Observatory, Japan	1621
1986 Jan 1	1.72	5.52	G. Emerson, E.E. Barnard Observatory, USA	127

Table 3: 1985 Dec 31.2 DE: Observation time, the calculated distance between the comet head and the end of the disconnected plasma tail, observatory and observers for the images 31 December 1985 through 1 January 1986.

Date	Hours (UT)	Distance (10^6 km)	Observer(s) Observatory	LSPN No.
1986 Feb 22	3.02	1.36	F. Van Wyk, LSPN Island Network, Sutherland	1781
	18.70	2.70	UKSTU, Royal Observatory/UKSTU, Australia	127

Table 4: 1986 Feb 21.7 DE: Observation time, the calculated distance between the comet head and the end of the disconnected plasma tail, observatory and observers for the images on 22 February 1986.

Date	Hours (UT)	Distance (10^6 km)	Observer(s) Observatory	LSPN No.
1986 Mar 2	0.00	2.62	W. Liller, University of Michigan/CTIO, Chille	1357
	11.48	2.71	W. Liller, University of Michigan/CTIO, Chille	1354
	11.76	2.74	W. Liller, University of Michigan/CTIO, Chille	1356
	12.04	2.75	W. Liller, University of Michigan/CTIO, Chille	1358

Table 5: 1986 Feb 28.7 DE: Observation time, the calculated distance between the comet head and the end of the disconnected plasma tail, observatory and observers for the images on 2 March 1986.

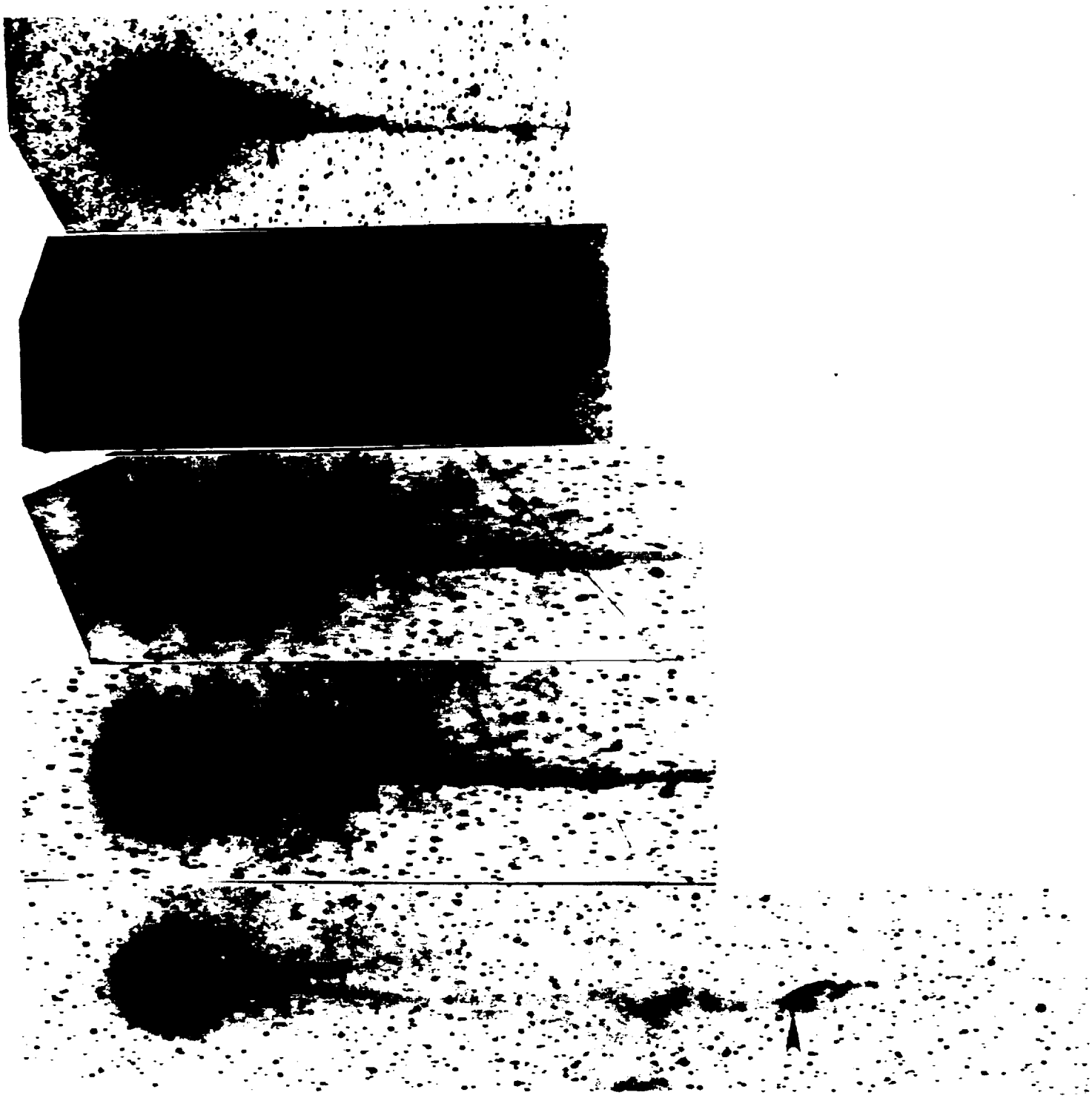

Trident Flight

ORIGINAL PAGE IS
OF POOR QUALITY

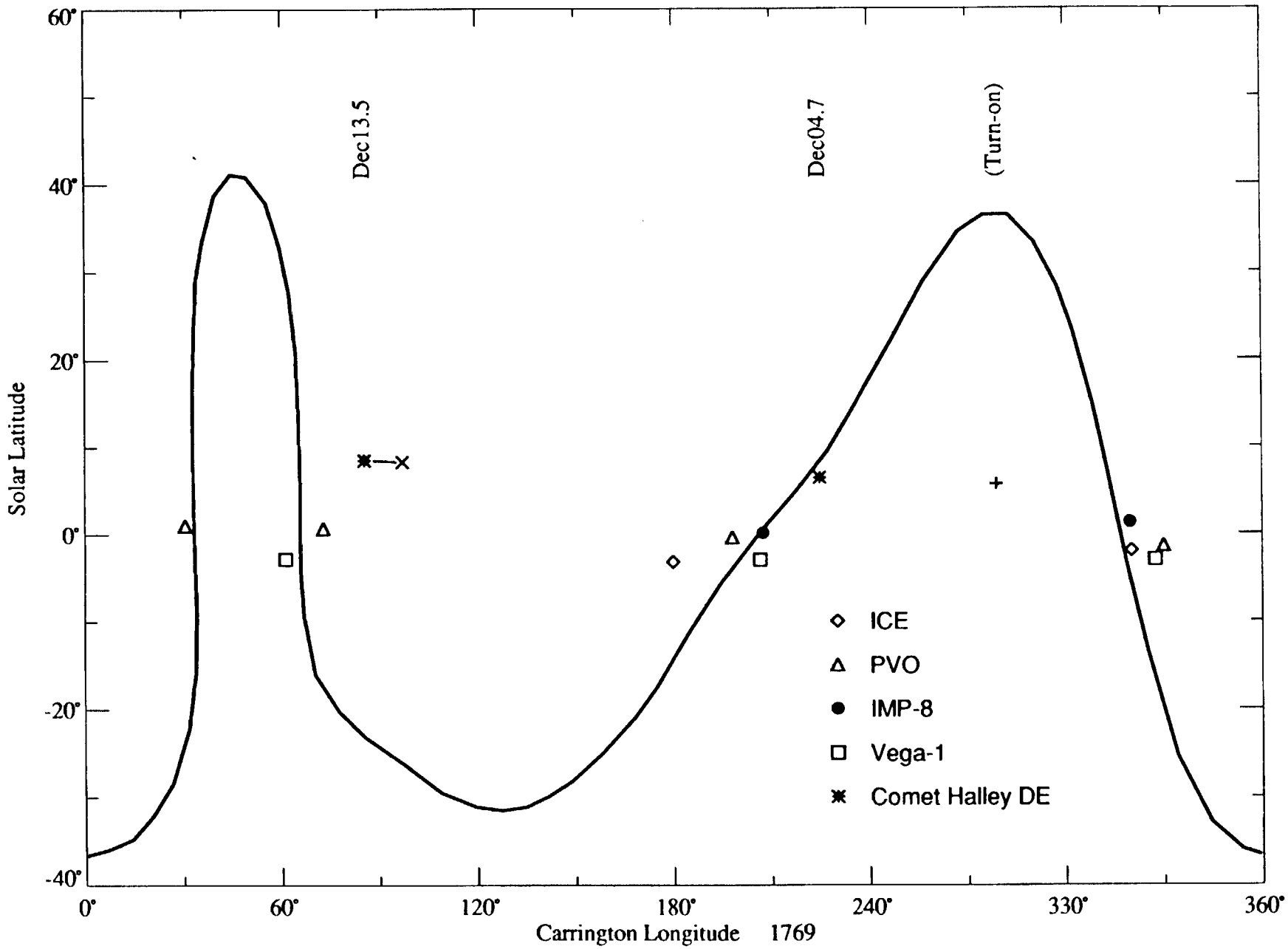
60°
40°
20°
0°
-20°
-40°
Solar Latitude
Dec13.5
Dec04.7
(Turn-on)
ICE
PVO
IMP-8
Vega-1
Comet Halley DE
0°
60°
120°
180°
240°
330°
360°
Carrington Longitude 1769

Yi et al / Fig. 2

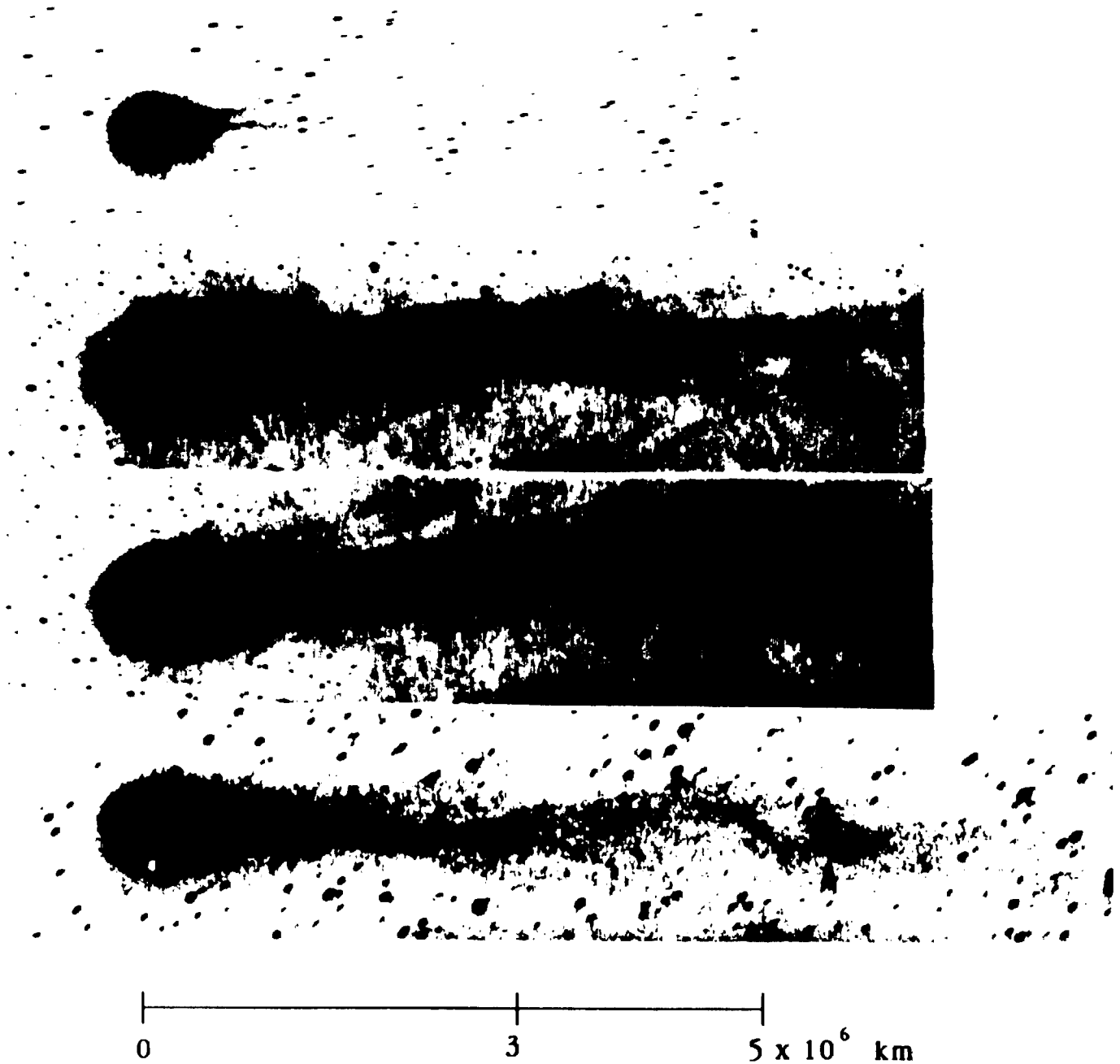

Yi et al / fig 3

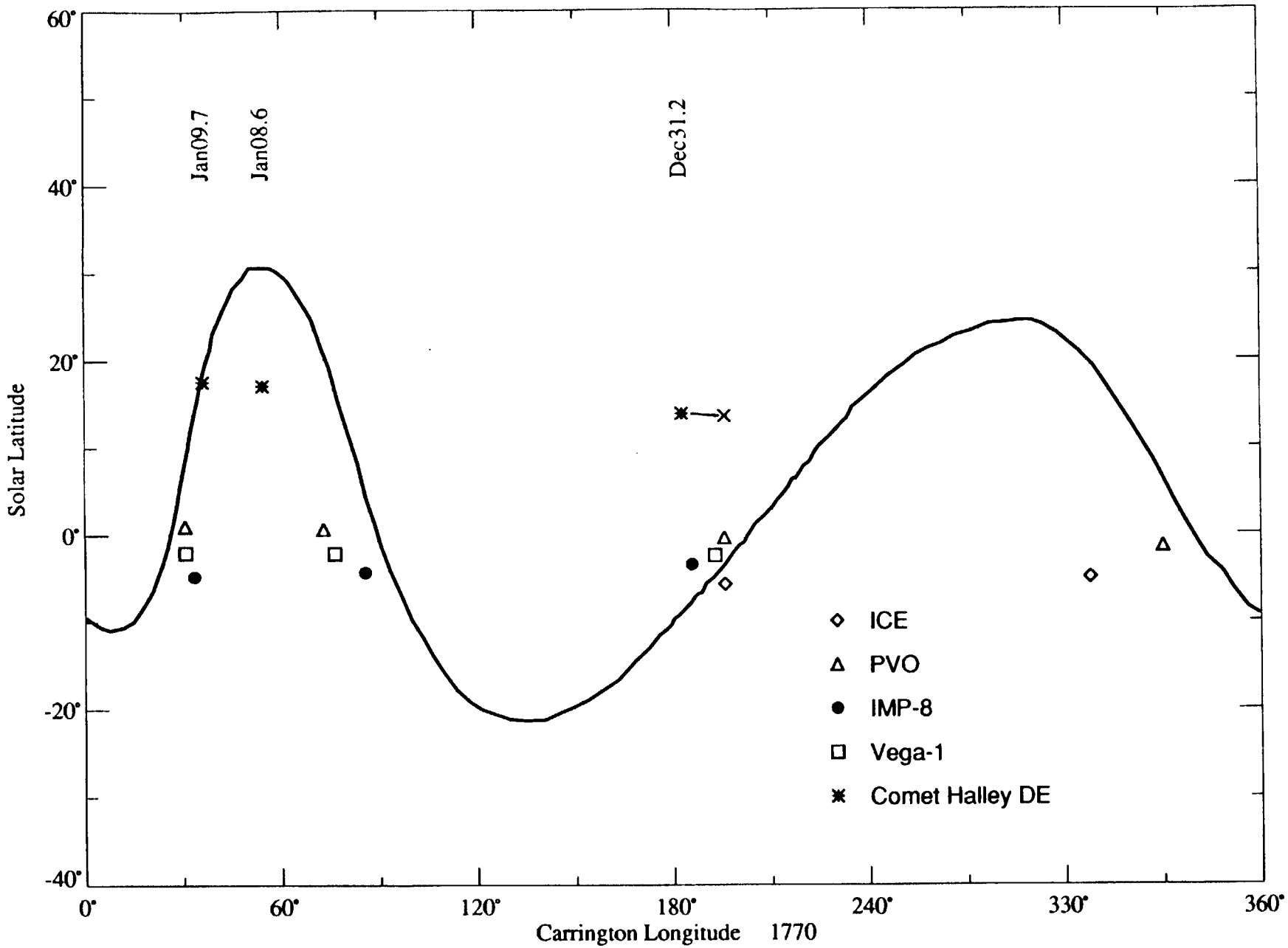
60°
40°
20°
0°
-20°
-40°
Solar Latitude
Jan09.7
Jan08.6
Dec31.2
ICE
PVO
IMP-8
Vega-1
Comet Halley DE
0°
60°
120°
180°
240°
330°
360°
Carrington Longitude 1770

4, et al/Fig 4

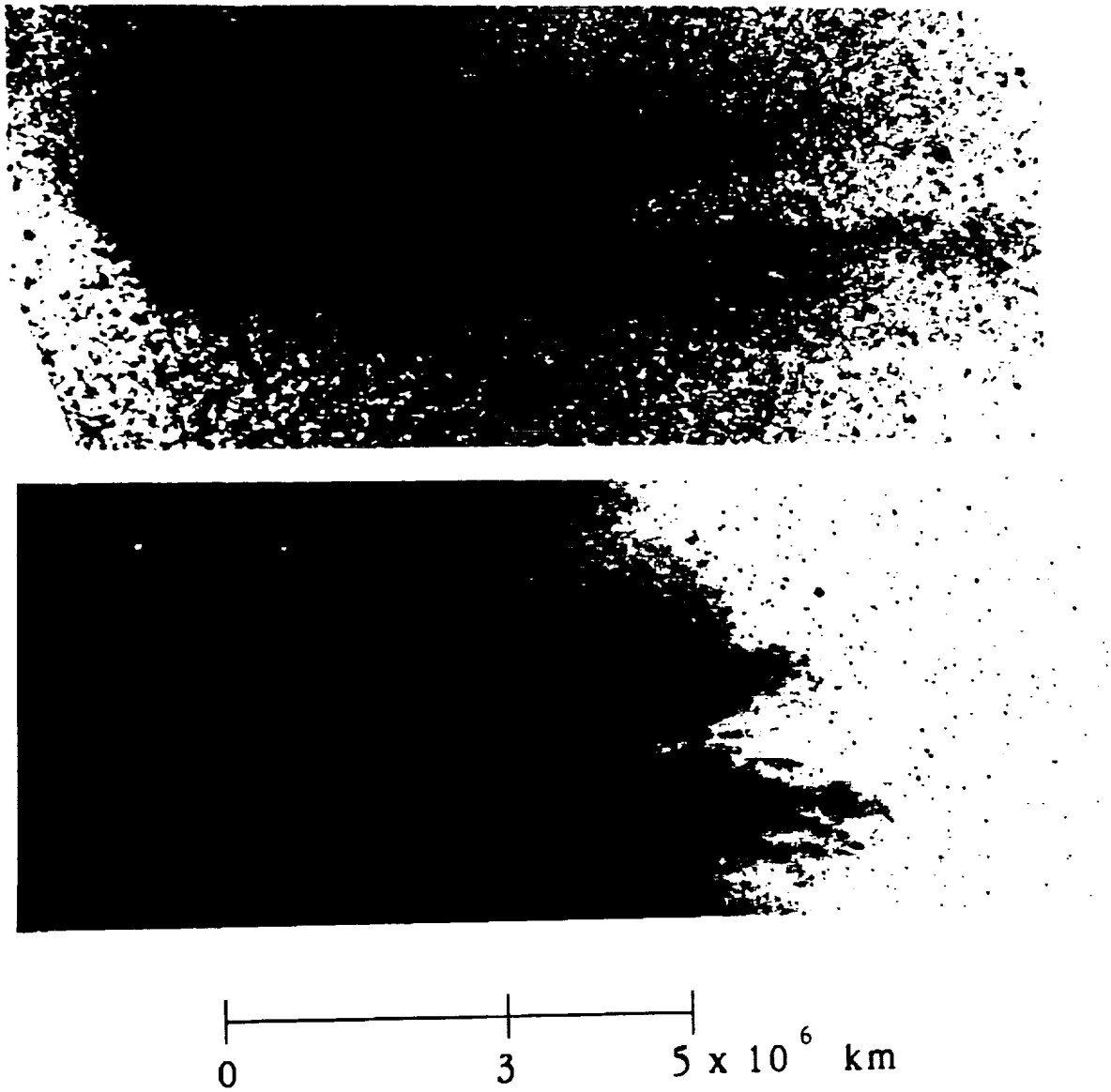

Fig. 5

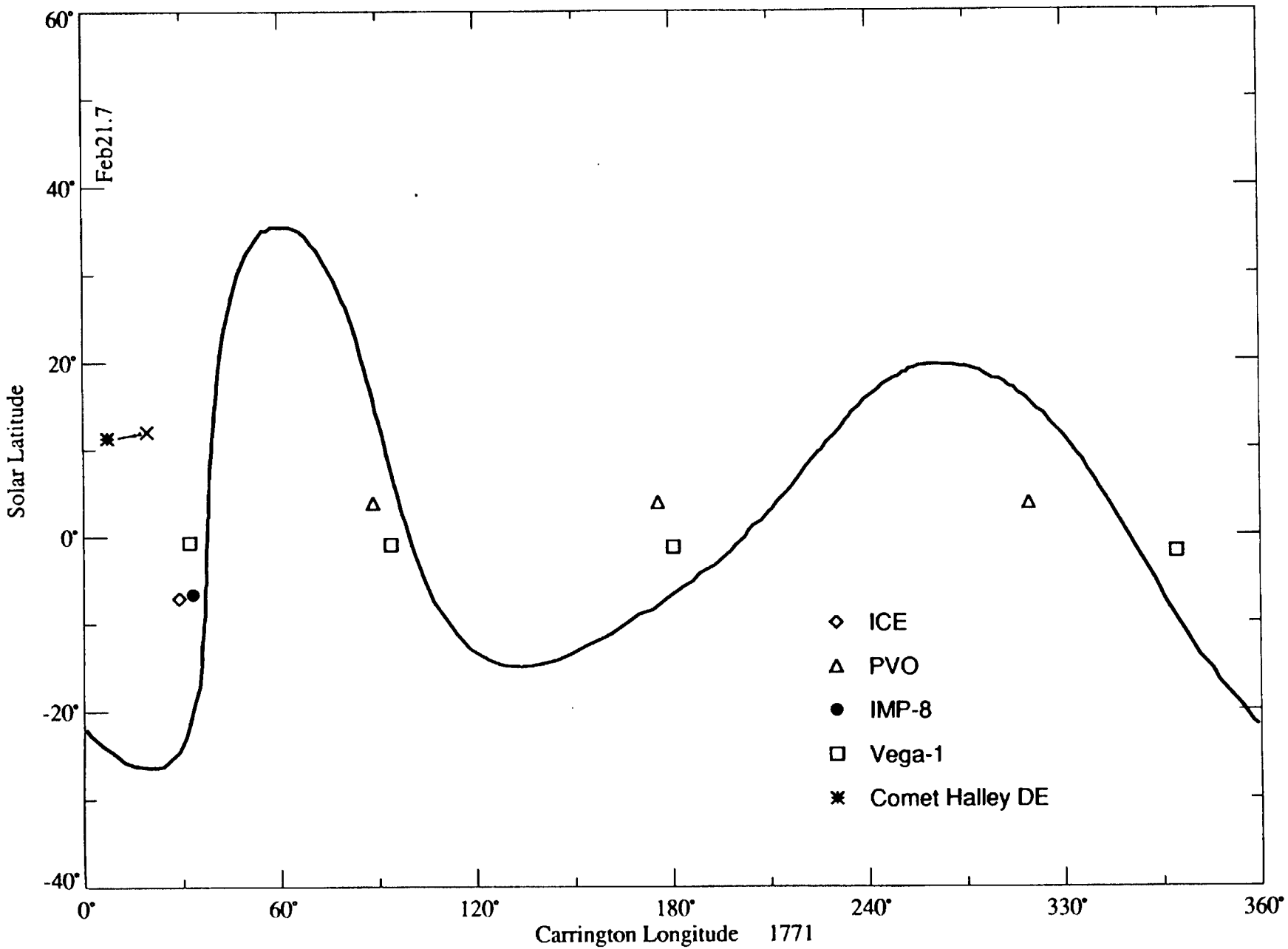
60°
40°
20°
0°
-20°
-40°
Feb21.7
Solar Latitude
0°
60°
120°
180°
240°
330°
360°
Carrington Longitude 1771
ICE
PVO
IMP-8
Vega-1
Comet Halley DE

Yi et al / Fig. 6

Yi et al / Fig

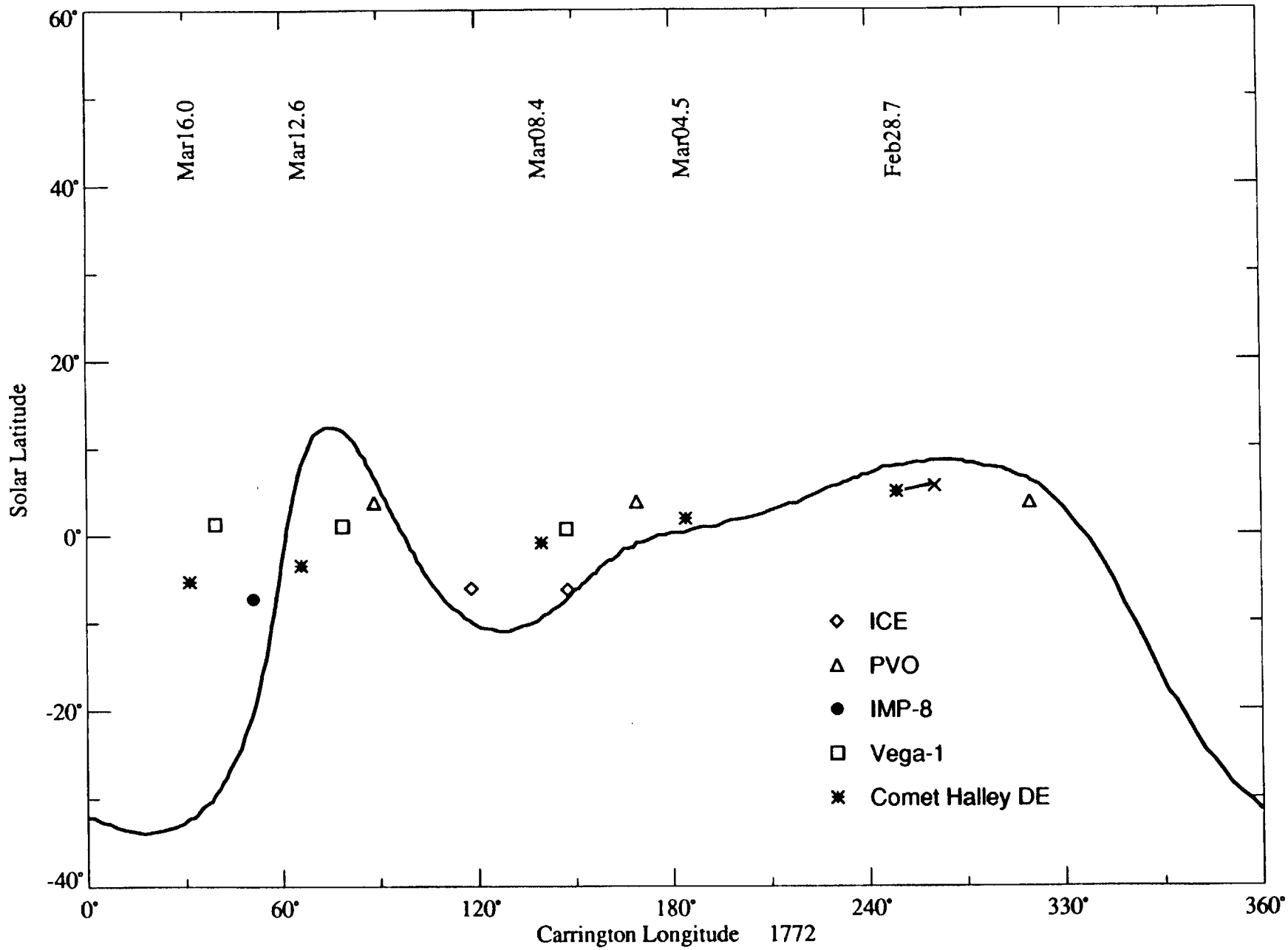
60°
40°
20°
0°
-20°
-40°
Solar Latitude
Mar16.0
Mar12.6
Mar08.4
Mar04.5
Feb28.7
ICE
PVO
IMP-8
Vega-1
Comet Halley DE
0°
60°
120°
180°
240°
330°
360°
Carrington Longitude 1772

Yi et al / Fig 8

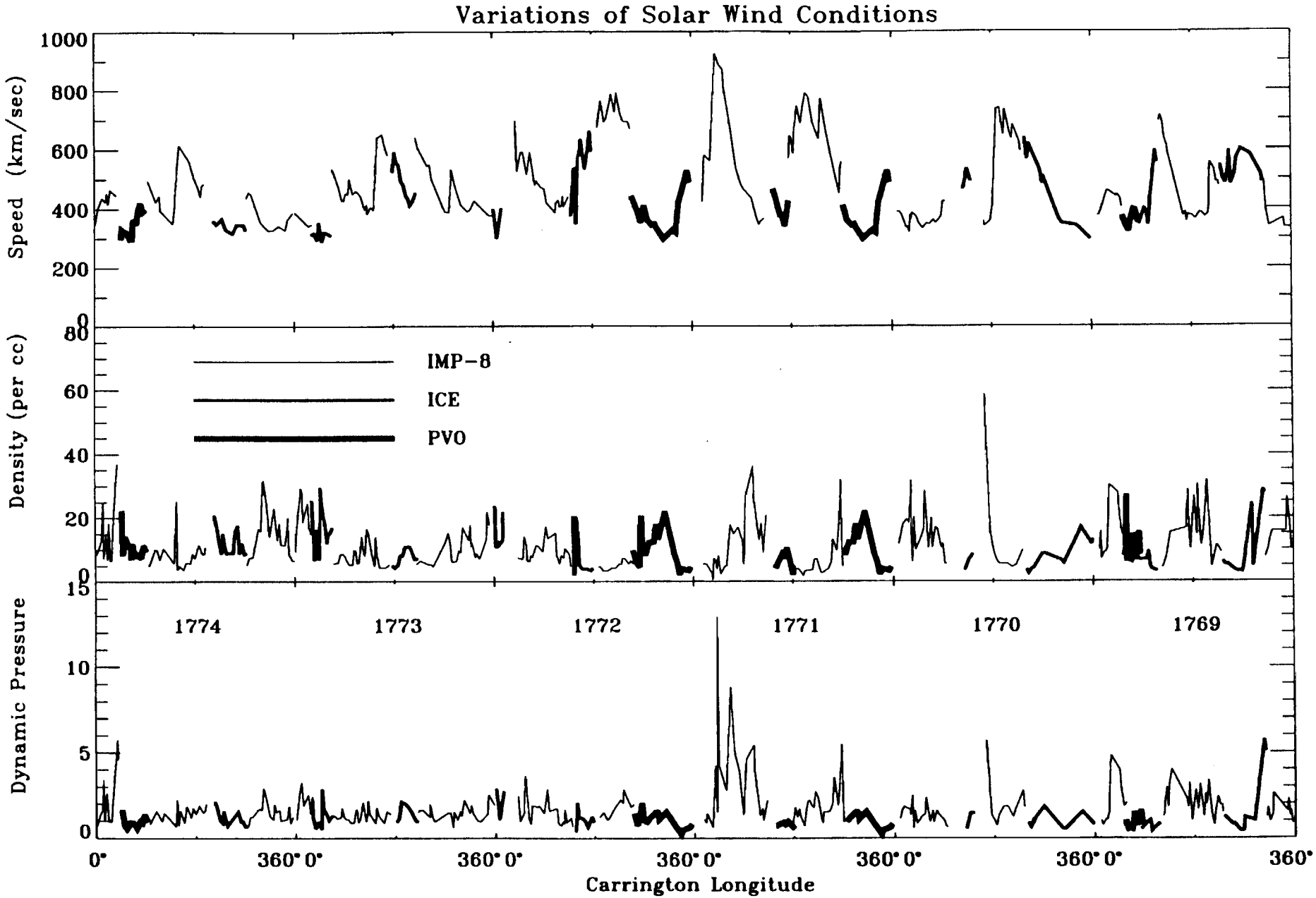
Variations of Solar Wind Conditions
Speed (km/sec)
1000
800
600
400
200
0
Density (per cc)
80
60
40
20
0
IMP-8
ICE
PVO
Dynamic Pressure
15
10
5
0
1774
1773
1772
1771
1770
1769
0°
360° 0°
360° 0°
360° 0°
360° 0°
360° 0°
360°
Carrington Longitude

Yi et al. / Fig. 9

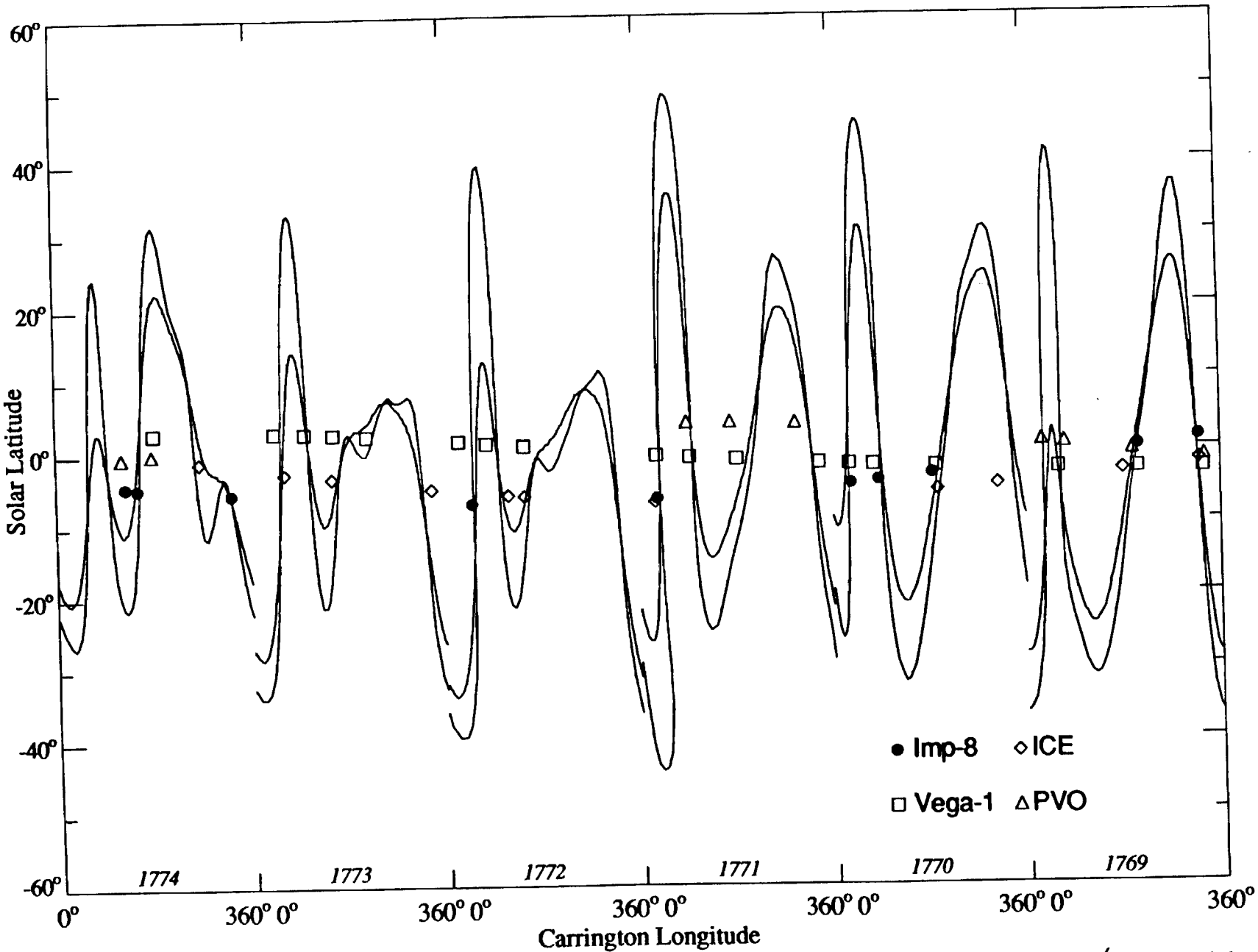

Yi et al./Fig. 10

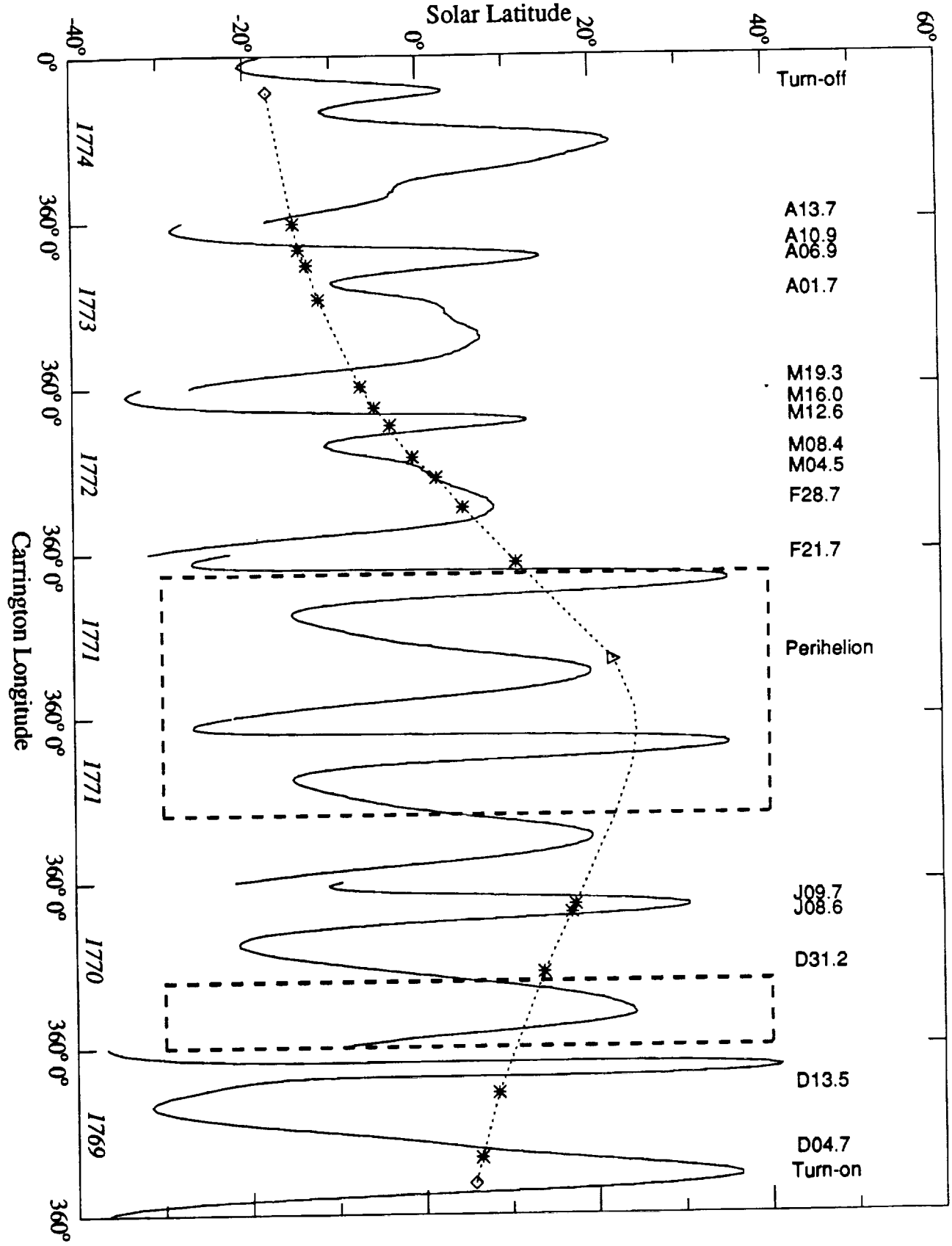

Yi et al. / Fig. 11

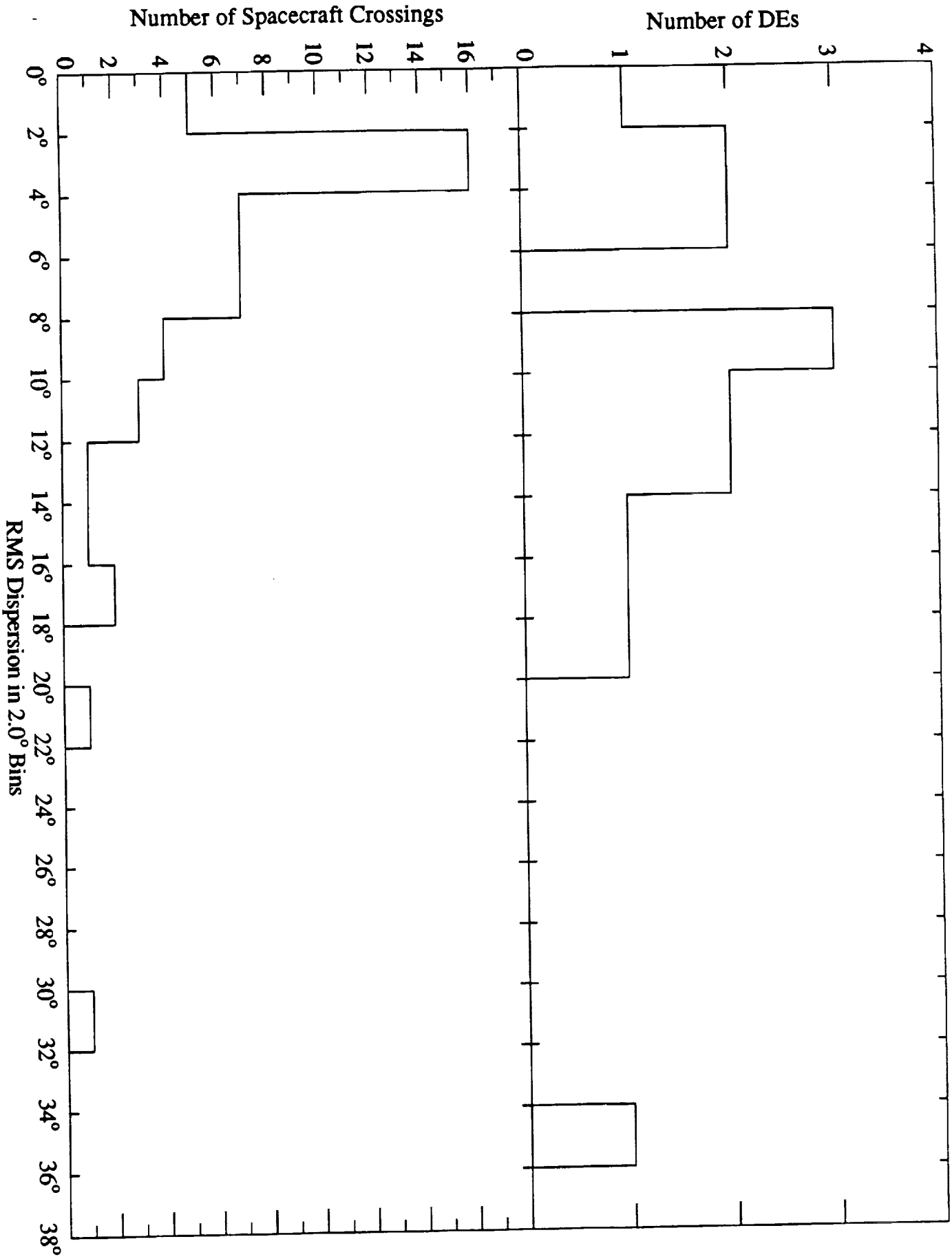

Yi et al. / Fig. 12

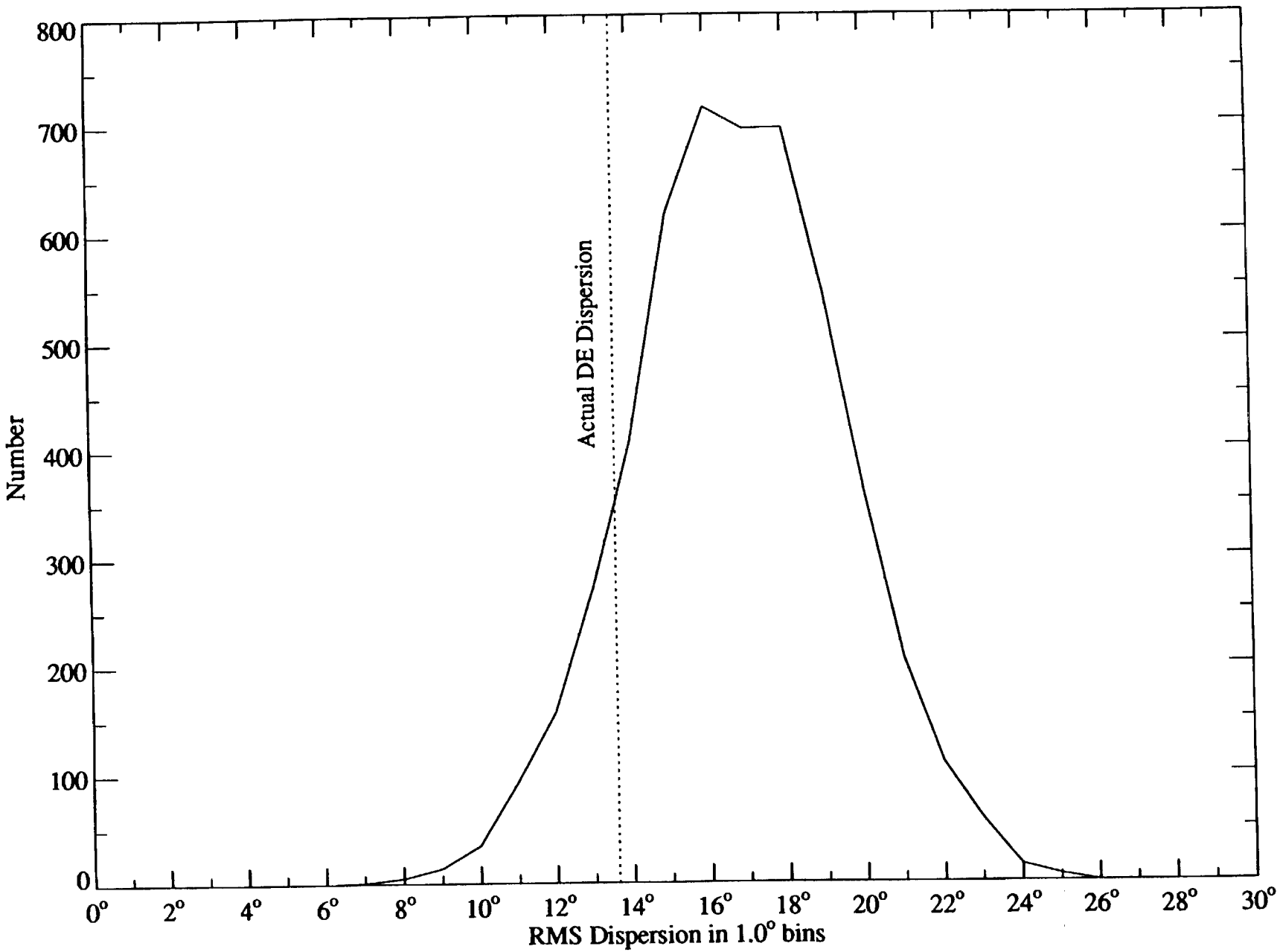

Yi et al. / Fig. 13

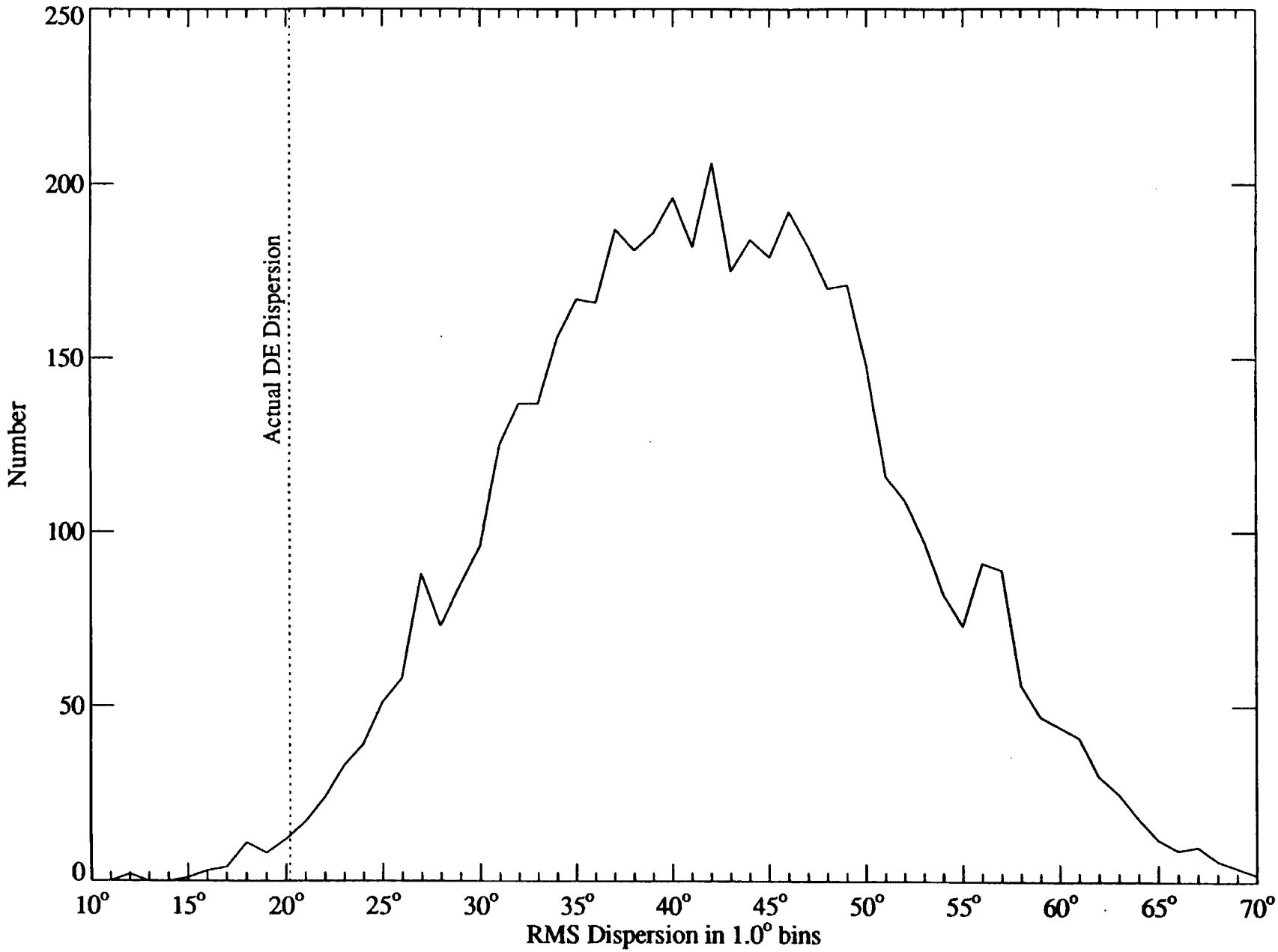

Yi et al. / Fig. 14

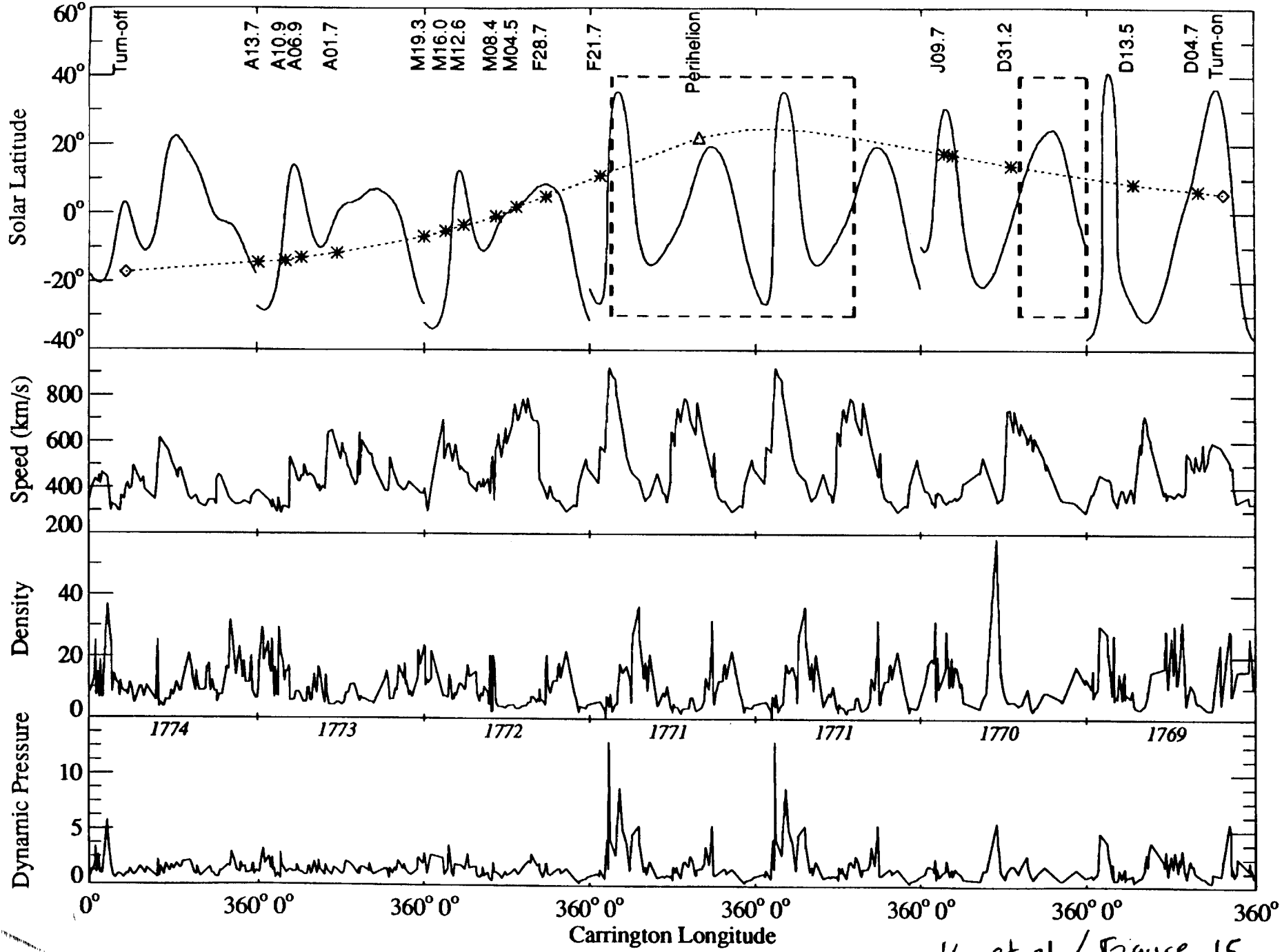

Li et al / Figure 15